Supplementary Information

Low-Threshold Room-Temperature Continuous-Wave Optical Lasing of Single-Crystalline Perovskite in a Distributed Reflector Microcavity

Cheng Tian, Tong Guo, Shiqi Zhao, Wenhao Zhai, Chaoyang Ge, Guangzhao Ran*

State Key Laboratory for Artificial Microstructure and Mesoscopic Physics, School of Physics, Peking University, Beijing 100871, China

1. Materials and experiments

Chemical materials and substrates: Lead bromide powder ($PbBr_2$, 99.99%) and methanaminium bromide powder (MABr, 99.99%) were purchased from Xi'an Polymer Light Technology Corporation (China); DMF (anhydrous, 99.8%) from Sigma Aldrich. All the materials were used as received. The double-side polished quartz substrates were purchased from Zhongnuo New Material Technology Corporation (China); distributed Bragg reflector (DBR) mirrors from Fujian CRYSTOCK Corporation (China). All the substrates were cleaned successively with acetone, ethanol and deionized water under sonication for 10 min and treated by O_2-plasma for 10 min.

Characterization of the thin film: The PL lifetime was measured by time-correlated single-photon counting (TCSPC) setup, by using pump laser source (PDL 800-D) and Module and Picosecond Event Timer (PicoHarp 300) from PicoQuant. We integrated the data of every sampling dots in a single piece of complete single-crystalline film as the data of PL lifetime of the film. X-ray diffraction (XRD) patterns of the perovskite thin films grown on a quartz sub-

*Corresponding author
URL: rangz@pku.edu.cn (Guangzhao Ran)

strate were measured by X-Pert3 powder diffraction system from PANalytical with a Cu tube operated at 40 kV and 40 mA. The surface morphology and cross-sectional images were taken by scanning electron microscope (Helios 600) from FEI Company with 10 kV acceleration voltage. The cross-sectional SEM image of $MAPbBr_3$ film on DBR substrate (the top DBR has been removed) is shown in Fig S1.

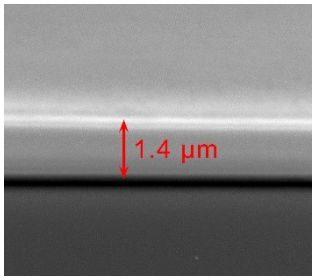

Fig. S1 The cross-sectional SEM image of $MAPbBr_3$ film on DBR substrate (the top DBR has been removed).

Optical spectroscopy characterization: In our handmade PL and laser measurement system, the pump sources were a nanosecond pulsed laser (Nd:YAG laser, frequency tripled, 355 nm, pulse width 8.0 ns, 1.0 kHz) and a continuous-wave semiconductor laser (405 nm). The excitation power was measured by a laser power meter from Thorlab Compony (S120VC). The light spot of the pump laser diode was focused on the center of the perovskite film by a 10x objective lens and the light emission of the devices was collected through a long-pass filter to deduct any residual light from the pump laser. The lasing spectra were recorded on a spectrometer (SR-500i, Andor Technology).

2. Coupled oscillator model

As discussed in the main text, to include the effect of exciton-photon, energy (E) and wavevector (k) have a dispersion relation as follow:

$$E(\omega, k) = \hbar\omega = \hbar ck/\sqrt{\varepsilon(\omega)}$$

The coupled oscillator model of dielectric function was used[1, 2] as:

$$\varepsilon(\omega) = \varepsilon_b \left(1 + \frac{\omega_L^2 - \omega_T^2}{\omega_T^2 - \omega^2 - i\omega\gamma}\right)$$

Where $\varepsilon_b = 4.7$ is the background dielectric constant [3], ω_T and ω_L are the transverse and longitudinal resonance frequencies of exciton and γ is the exciton damping. The parameters $\hbar\omega_T = 2.303\ eV$ and $\hbar\gamma = 59\ meV$ were taken from reported values [4]. The dispersion curve was fitted by only one parameter, $\hbar\omega_L$. With the dielectric function and eigenmode solver simulation of waveguide modes (MODE Solutions, Lumerical), the effective refractive index $n_{eff}(\lambda)$ was obtained at different wavelengths for the fundamental mode. Then, we have the relations:

$$k_z = \frac{2\pi n_{eff}}{\lambda}$$
$$E = \frac{hc}{\lambda}$$

k_z of the resonant peaks can be placed with integral multiples of π/h, where h is the thickness of the film. The dispersion curve was fitted as shown in Fig. 2(c) and we obtained the longitudinal-transverse splitting energy $\Delta E_{LT} = \hbar\omega_L - \hbar\omega_T = 30\ meV$.

The mode of the film we calculated concentrate most energy in the gain medium, so we used the volume of the film instead of the effective volume approximately. The exciton-photon coupling strength is expressed as vacuum Rabi splitting energy Ω, which was used as [1, 2]:

$$\Omega = \sqrt{\hbar\omega_L^2 - \hbar\omega_T^2} \approx \sqrt{2\Delta E_{LT} \cdot \hbar\omega_T}$$

Then, we obtained vacuum Rabi splitting energy $\Omega = 372\ meV$.

3. Rate equation analysis

To better understand the lasing behavior of our devices, we performed a conventional rate equations analysis [5, 6]. The dynamics of the carrier density $N(t)$ and photon density $N_p(t)$ that couple into a specific mode can be

represented as follow:

$$\frac{dN}{dt} = \frac{\eta_p P}{\hbar\omega V} - \frac{N}{\tau_{PL}} - v_g g N_p$$
$$\frac{dN_p}{dt} = \Gamma v_g (g - g_{th}) N_p + \Gamma\beta\frac{N}{\tau_r}$$

Where η_p is the fraction of pump power absorbed by the perovskite film which we simply chose $\eta_p = 1$ because of the high absorption coefficient. P is the pump power and V is the volume of gain medium, so P/V is the pump power density times the thickness of gain medium which is 1.36 μm. $\hbar\omega$ is the energy of the pump beam. τ_{PL} is the PL lifetime, which is set to be 426 ns from the PL lifetime measurement in Fig. 1(c) and τ_r is the spontaneous emission lifetime. Here we adopted the value of 1000 ns according to the reported longest PL lifetime [7, 8]. Γ is the optical confinement factor which we set $\Gamma = 1$, because the DBR mirrors with high reflectivity had extremely strong optical confinement on the optical mode we cared about. v_g is the group velocity, and from mode analysis using Lumerical Mode solutions we obtained $v_g = c/2.29$ for CW pumped lasing and $v_g = c/2.285$ for pulsed pumped lasing, where c is the light velocity in vacuum. g_{th} is the equivalent threshold gain, and β is the spontaneous emission factor. g is the gain and a linear relation between gain g and carrier density N is assumed in the active region, $g(N) = \alpha(N - N_{tr})$, where α is a material constant, and N_{tr} is the transparency carrier density, which is approximated to zero for simplicity [6].

For the CW pumped lasing, all time differential terms are zero. The carrier density is eliminated and the rate equations are reduced to a algebraic equation as follow:

$$\frac{\eta_p P}{\hbar\omega V}\left(\frac{\beta}{\tau_r} + v_g\alpha N_p\right) = v_g g_{th} N_p \left(\frac{1}{\tau_{PL}} + v_g\alpha N_p\right)$$

We fitted the algebraic equation with the data points and obtained the spontaneous emission factor $\beta = 0.08$, as shown in Fig. 4(d).

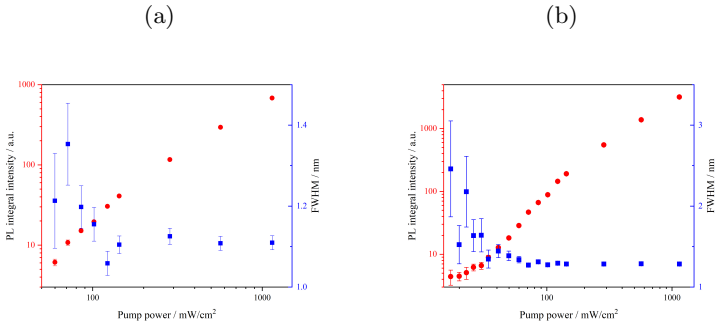

Fig. S2 (a) The intensity and FWHM of 547 nm peak change along with increasing pump fluences in a logarithmic coordinate system. (b) The intensity and FWHM of 591 nm peak change along with increasing pump fluences in a logarithmic coordinate system.

4. Analysis of the side peaks in CW pumping case

The integral intensity and FWHM of the peaks at 547 and 591 nm are shown in Fig. S2. The peak at 547 nm is much weaker and undetectable under the pump fluences below 50 mW/cm^2. From the remaining data under higher pump fluences shown in Fig. S2(a), no obvious nonlinear change is be observed. The FWHM is 1.1 nm at the highest pump fluence.

On the other hand, the peak at 591 nm can be fitted well by Gaussian curves. A visible S-shaped curve is observed in Fig. S2(b). The nonlinear change of the intensity and the narrowing of linewidth appear simultaneously under the pump fluence of around 34 mW/cm^2. This peak is near the edge of the high reflection zone as shown in Fig. 4(b) so that the final FWHM is 1.3 nm, which is larger than the one of the center peak.

References

[1] S. Zhang, Q. Shang, W. Du, J. Shi, Z. Wu, Y. Mi, J. Chen, F. Liu, Y. Li, M. Liu, et al., Strong exciton–photon coupling in hybrid inorganic–organic perovskite micro/nanowires, Advanced Optical Materials 6 (2) (2018) 1701032.

[2] L. K. van Vugt, B. Piccione, C.-H. Cho, P. Nukala, R. Agarwal, One-dimensional polaritons with size-tunable and enhanced coupling strengths in semiconductor nanowires, Proceedings of the National Academy of Sciences 108 (25) (2011) 10050–10055.

[3] M. Sendner, P. K. Nayak, D. A. Egger, S. Beck, C. Müller, B. Epding, W. Kowalsky, L. Kronik, H. J. Snaith, A. Pucci, et al., Optical phonons in methylammonium lead halide perovskites and implications for charge transport, Materials Horizons 3 (6) (2016) 613–620.

[4] H. Kunugita, T. Hashimoto, Y. Kiyota, Y. Udagawa, Y. Takeoka, Y. Nakamura, J. Sano, T. Matsushita, T. Kondo, T. Miyasaka, et al., Excitonic feature in hybrid perovskite ch3nh3pbbr3 single crystals, Chemistry Letters 44 (6) (2015) 852–854.

[5] S. Chen, C. Zhang, J. Lee, J. Han, A. Nurmikko, High-Q, low-threshold monolithic perovskite thin-film vertical-cavity lasers, Advanced Materials 29 (16) (2017) 1604781.

[6] Y. Ye, Z. J. Wong, X. Lu, X. Ni, H. Zhu, X. Chen, Y. Wang, X. Zhang, Monolayer excitonic laser, Nature Photonics 9 (11) (2015) 733.

[7] D. Shi, V. Adinolfi, R. Comin, M. Yuan, E. Alarousu, A. Buin, Y. Chen, S. Hoogland, A. Rothenberger, K. Katsiev, et al., Low trap-state density and long carrier diffusion in organolead trihalide perovskite single crystals, Science 347 (6221) (2015) 519–522.

[8] Y. Liu, Y. Zhang, K. Zhao, Z. Yang, J. Feng, X. Zhang, K. Wang, L. Meng, H. Ye, M. Liu, et al., A 1300 mm^2 ultrahigh-performance digital imaging assembly using high-quality perovskite single crystals, Advanced Materials 30 (29) (2018) 1707314.